Cloud Radiative Forcing of the Arctic Surface: The Influence of Cloud Properties, Surface Albedo, and Solar Zenith Angle

MATTHEW D. SHUPE

Science and Technology Corporation, NOAA/Environmental Technology Laboratory, Boulder, Colorado

JANET M. INTRIERI

NOAA/Environmental Technology Laboratory, Boulder, Colorado

(Manuscript received 11 March 2003, in final form 5 August 2003)

ABSTRACT

An annual cycle of cloud and radiation measurements made as part of the Surface Heat Budget of the Arctic (SHEBA) program are utilized to determine which properties of Arctic clouds control the surface radiation balance. Surface cloud radiative forcing (CF), defined as the difference between the all-sky and clear-sky net surface radiative fluxes, was calculated from ground-based measurements of broadband fluxes and results from a clear-sky model. Longwave cloud forcing (CF_{LW}) is shown to be a function of cloud temperature, height, and emissivity (i.e., microphysics). Shortwave cloud forcing (CF_{SW}) is a function of cloud transmittance, surface albedo, and the solar zenith angle. The annual cycle of Arctic CF reveals cloud-induced surface warming through most of the year and a short period of surface cooling in the middle of summer, when cloud shading effects overwhelm cloud greenhouse effects. The sensitivity of CF_{LW} to cloud fraction is about 0.65 W m^{-2} per percent cloudiness. The sensitivity of CF_{SW} to cloud fraction is a function of insolation and ranges over 0–1.0 W m^{-2} per percent cloudiness for the sun angles observed at SHEBA. In all seasons, liquid-containing cloud scenes dominate both LW and SW radiative impacts on the surface. The annual mean CF_{LW} (CF_{SW}) for liquid-containing and ice-only cloud scenes is 52 (−21) and 16 (−3) W m^{-2}, respectively. In the LW, 95% of the radiatively important cloud scenes have bases below 4.3 km and have base temperatures warmer than −31°C. The CF_{LW} is particularly sensitive to LWP for LWP < 30 g m^{-2}, which has profound implications in the winter surface radiation balance. The CF_{SW} becomes more negative as surface albedo decreases and at higher sun elevations. Overall, low-level stratiform liquid and mixed-phase clouds are found to be the most important contributors to the Arctic surface radiation balance, while cirrus clouds and diamond dust layers are found to have only a small radiative impact on the Arctic surface.

1. Introduction

Clouds play a complex and important role in the earth's radiative balance, particularly in the Arctic where a dry atmosphere and high surface albedo amplify cloud radiative influences. Furthermore, Arctic clouds play significant roles in the influential but not well understood ice–albedo and cloud–radiation feedback mechanisms (Curry et al. 1996). Due to these feedbacks and the presence of sea ice, the Arctic is expected to be very sensitive to global changes in climate (Meehl and Washington 1990); however, our knowledge of how changes may affect Arctic clouds, sea ice, surface temperature, and atmospheric moisture is limited. For example, modifications in surface temperature, cloud condensation nuclei concentration, and/or low-level atmospheric stability will undoubtedly coincide with changes in cloudiness and cloud characteristics such as water content, particle size, and precipitation amount. Understanding these potential changes is critical since Arctic clouds are considerably important in the annual onset of snowmelt (Zhang et al. 1996), in the yearly melting and formation of sea ice (Maykut and Untersteiner 1971), and in determining atmospheric heating rate profiles.

Clouds participate in two competing manners in the surface radiation budget: warming the surface through the emission of longwave (LW) radiation and cooling the surface by shading the incident shortwave (SW) radiation. Clouds are especially important in the Arctic LW budget because of the dryness of the Arctic atmosphere, relative to lower latitudes, which produces relatively less clear-sky atmospheric emission. Due to frequent temperature inversions, Arctic clouds often emit at temperatures that are warmer than the underlying surface. The role of clouds in the Arctic SW budget is variable over the annual cycle due to the long polar summer and winter and the highly reflective surface.

Corresponding author address: Matthew Shupe, NOAA/Environmental Technology Laboratory, R/ET6, 325 Broadway, Boulder, CO 80305.
E-mail: Matthew.Shupe@noaa.gov

Sun angle also impacts the cloud–SW radiation relationship, but its exact role is unclear (Minnett 1999; Curry et al. 1996).

The balance of these SW and LW effects is referred to as cloud radiative forcing (CF), with positive CF indicating that clouds warm the surface relative to clear skies, and negative CF indicating that clouds cool the surface. Using surface-based measurements, Intrieri et al. (2002a) showed that over the permanent ice pack in the western Arctic basin, clouds warm the surface through most of the year except for a short period in midsummer when their albedo effect outweighs their greenhouse effect. Other studies have made similar observations in the Arctic based on satellite measurements (e.g., Schweiger and Key 1994), surface observations (e.g., Cogley and Henderson-Sellers 1984; Walsh and Chapman 1998), and model studies (e.g., Curry and Ebert 1992), although the spread in results is significant in terms of total surface heat budgets.

Since clouds are so intimately involved in the Arctic surface radiation budget, it is necessary to more clearly understand how they interact with radiation and to distinguish which particular cloud properties are most important. In effect, we need to answer the question: *What makes an Arctic cloud radiatively important?* An appropriate answer to this question is essential in order to accurately model cloud–radiation interactions.

Modeling is the most practical method to understand widespread climate change, especially in the Arctic where observations are hindered by the extreme conditions encountered there. One model study suggested that an increase in atmospheric greenhouse gases would lead to increases in total cloudiness and a subsequent warming of the Arctic surface (Miller and Russell 2002). Climate change studies of this nature, which have the potential to provide important results for climate prediction, are only possible if climate models can accurately portray the interactions of clouds, radiation, the atmosphere, and the surface. Current model results, however, are highly variable, particularly in the Arctic and in dealing with Arctic clouds. Tao et al. (1996) and Chen et al. (1995), in documenting an intercomparison of 19 general circulation models (GCMs), showed a variation of greater than 50% in total cloudiness predicted by the different models, with some models showing an opposite annual cycle trend from surface observations. A more recent comparison of 13 GCMs showed moderate improvements in simulating cloudiness; however, large deficiencies still exist in modeling the cloud–radiation relationship (Walsh et al. 2002). To improve and assure model quality, observational data must be incorporated into any parameterization development. Therefore, intensive observational programs, such as the Surface Heat Budget of the Arctic Ocean (SHEBA) program (Perovich et al. 1999; Uttal et al. 2002), have recently focused on improving observational datasets on the cloud–radiation and ice–albedo feedbacks in the Arctic.

The SHEBA field camp was based on an icebreaking ship that was frozen into, and drifted with, the permanent ice pack in the Beaufort and Chukchi Seas north of Alaska from October 1997 to October 1998. An exceptional quality of the SHEBA program was that, for the first time, a wide range of Arctic ice, atmosphere, and ocean observations were made over a full annual cycle. The SHEBA experiment included an extensive suite of state-of-the-art instruments capable of measuring all components of the surface heat budget. Here, we examine an annual cycle of cloud measurements from lidar and radar (Intrieri et al. 2002b) and broadband radiation measurements (Persson et al. 2002) to identify the characteristics of clouds that are important in the Arctic surface radiation balance. Intrieri et al. (2002a) presented average surface cloud forcing information for SHEBA, with an annual average LW and SW CF of 38 and -9 W m^{-2}, respectively. Here, we expand upon this previous work by examining the qualities of clouds that make them radiatively important to the surface. Namely, we explore cloud temperature, height, phase, and liquid water path and how these factors influence the radiative balance. Furthermore, we examine how solar zenith angle and surface albedo influence the effect that clouds have on surface radiation. A simple radiative flux model and sensitivity relationships are used to qualitatively illustrate the impact of changes to various parameters on the radiation balance.

2. Instruments and data considerations

a. Instruments and measurements

Upwelling and downwelling radiometric fluxes were measured at SHEBA using broadband radiometers (Persson et al. 2002). Eppley Precision Infrared Radiometer hemispheric flux pyrgeometers were used to measure LW radiation, and Precision Solar Pyranometers were used to measure SW radiation. Estimated uncertainties for the net surface fluxes are 4.5% for SW (with a negative bias of a few W m^{-2}) and ± 4 W m^{-2} for LW (Intrieri et al. 2002a). All radiation measurements used in this dataset were hourly averages.

Observations of cloud presence and base height were made at SHEBA by a combination of lidar and radar measurements. The Depolarization and Backscatter Unattended Lidar (DABUL; Alvarez et al. 1998) measured profiles of returned power and depolarization ratio for 9 months of the SHEBA year. The Millimeter Cloud-Radar (MMCR; Moran et al. 1998) operated for over 11 months of the SHEBA year and provided profiles of radar reflectivity. The collocated measurements from the DABUL and the MMCR were combined to give a comprehensive, time–height view of cloudiness at SHEBA on an hourly time scale. For this dataset, a cloud was considered to be present if either instrument observed a hydrometeor return. Additional details on these in-

struments and the combined cloud dataset are presented in Intrieri et al. (2002b).

Column-integrated liquid water path (LWP) was derived from brightness temperatures measured by the microwave radiometer (MWR) operated by the Atmospheric Radiation Measurement Program (ARM; Stokes and Schwartz 1994) at SHEBA. The LWP retrievals are described by Westwater et al. (2001), who estimate the retrieval uncertainty to be about 25 g m^{-2}.

Profiles of temperature and relative humidity were measured by a GPS/LORAN atmospheric sounding radiosonde system. Soundings were made daily at 1200 and 2400 UTC for the entire SHEBA year, with additional soundings made at 0600 and 1800 UTC during periods of April through July 1998. Profiles were considered to be instantaneous at the time of the radiosonde launch, under the assumption that the radiosonde drift roughly follows the drift of the cloud scene observed by the vertically pointing instruments at the time of the launch. Uncertainties in measured temperatures are 0.2°C; however, the uncertainty that arises from interpolating in time is somewhat larger. Interpolated sounding data were used as model input and along with lidar/radar cloud boundary measurements to determine cloud temperature.

b. Identifying the presence of liquid water

The DABUL and MWR provide independent measurements of whether or not liquid exists in the vertical column. Each instrument has its limitations, however, which preclude our ability to fully characterize the phase of all clouds observed at SHEBA. For the MWR, retrievals of LWP greater than 25 g m^{-2} (the retrieval uncertainty) clearly indicate the presence of liquid but do not distinguish its vertical location. For the DABUL, depolarization ratios less than 0.11 indicate liquid water at a given vertical location (Intrieri et al. 2002b), but the lidar signal attenuates in optically thick clouds, preventing measurements in higher cloud layers. At SHEBA, the DABUL detected liquid in the vertical column 72% of the time clouds were present and 49% of all time, while the MWR showed a significant level of liquid for these same quantities 50% and 41% of the time, respectively. Thus, these two techniques for identifying liquid do not always agree, and the disagreement is largely due to the high uncertainty in the MWR LWP retrievals. For times when DABUL did not detect liquid, the MWR LWP values are almost always below the uncertainty threshold (Fig. 1). For times when DABUL detected liquid, the distribution of LWPs shows many large and positive values, but also reveals that a significant portion (~40%) of the values fall below the liquid detection threshold. Here, the atmosphere is considered to contain cloud liquid in some amount if either instrument indicates liquid.

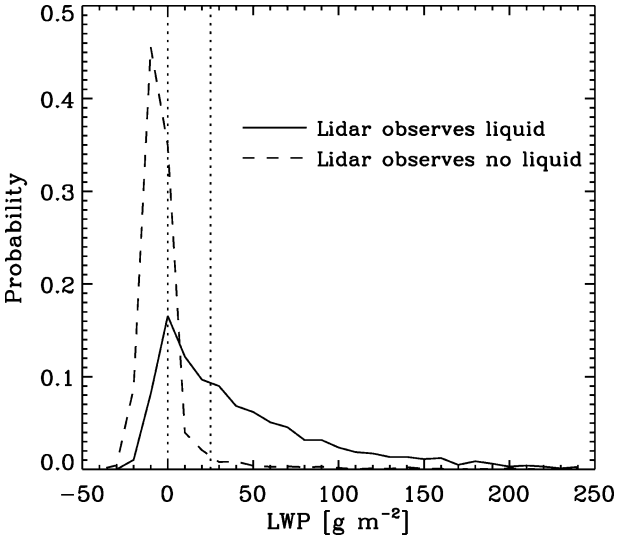

FIG. 1. Probability distribution functions of microwave-radiometer-derived LWP for time periods when the lidar observed liquid and no liquid in the atmospheric column. The dotted vertical lines identify LWP = 0 g m^{-2} and the LWP retrieval uncertainty of 25 g m^{-2}.

3. Cloud radiative forcing

Cloud radiative forcing is defined as the radiative impact that clouds have on the atmosphere, surface, or top-of-the-atmosphere (TOA) relative to clear skies. Here, we are interested in the role clouds play at the surface. The LW, SW, and total surface cloud forcing parameters are given as (Ramanathan et al. 1989)

$$\mathrm{CF}_{\mathrm{LW}} = F(A_c) - F(0), \tag{1a}$$

$$\mathrm{CF}_{\mathrm{SW}} = Q(A_c) - Q(0), \tag{1b}$$

$$\mathrm{CF} = \mathrm{CF}_{\mathrm{LW}} + \mathrm{CF}_{\mathrm{SW}}, \tag{1c}$$

where A_c is the cloud fraction, F and Q are the net surface LW and SW fluxes, respectively; the first and second terms in (1a) and (1b) are for all-sky and equivalent clear-sky conditions, respectively, and all fluxes are defined as positive downwards. The equivalent clear sky terms, according to these definitions, are considered to be the net surface fluxes neglecting all direct cloud effects. A negative cloud forcing indicates that clouds reduce the amount of radiation at the surface (i.e., a cooling effect), while a positive cloud forcing indicates surface warming.

a. A model for surface cloud forcing

In order to investigate the role of cloud and environmental properties in surface cloud forcing, (1) can be expanded using first-order atmospheric radiative flux models. The equations provided in this section are not intended to be fully quantitative but rather to act as qualitative tools to identify radiatively important properties. The models also provide a means for understand-

ing how the surface radiation balance may respond to changes in these properties.

The upwelling, surface emission, components of both all-sky and clear-sky net LW surface fluxes approximately cancel when calculating CF_{LW} with (1a); therefore, only the downwelling fluxes are considered here. The assumption of similar surface emission (or temperature) under clear and cloudy skies is most appropriate when considering the instantaneous effect of clouds on the surface, as is done here. The downwelling clear-sky LW flux is due to emission by aerosols and atmospheric gases. With the addition of a cloud layer, the LW flux becomes the sum of transmitted atmospheric emission above the cloud layer (which is mostly absorbed by the cloud), emission from the cloud itself (which is partially absorbed by the below-cloud atmosphere), emission from the atmosphere below the cloud, and radiation that is reflected downward by the cloud. To illustrate this radiative system, we consider the atmosphere divided into three slabs: the above-cloud atmosphere, the cloud layer, and the below-cloud atmosphere. Each layer has an effective temperature and broadband transmittance. We make the assumption that the temperature profile is independent of the cloud presence. Based on this generalized radiative transfer model, the clear and cloudy sky downwelling LW surface fluxes are given by

$$F^{\downarrow}(0) = t_{bl}\sigma T_a^4 + \sigma T_{bl}^4, \tag{2a}$$

$$F^{\downarrow}(A_c = 1) = t_{bl}(1 - \varepsilon_c)\sigma T_a^4 + t_{bl}\varepsilon_c\sigma T_c^4 + \sigma T_{bl}^4 + \mathrm{Re}, \tag{2b}$$

where T is temperature, t is broadband transmittance, ε is broadband emissivity, σ is the Stefan–Boltzmann constant, and the subscripts c, a, and bl denote the cloud, the above-cloud atmosphere, and the below-cloud atmosphere, respectively. Since cloud IR reflectance is small compared to cloud emission (Smith et al. 1993), the cloud reflectance term, Re, can be neglected. Cloud emissivity is then related to cloud LW transmittance via $\varepsilon_c = 1 - t_{cl}$, where the cloud transmittance is $t_{cl} = \exp(-\tau_{cl})$, and τ_{cl} is the cloud LW absorption optical depth, which is related to microphysical properties. Thus, to a first-order approximation, CF_{LW} is the contribution to the downwelling flux from cloud emission minus the radiation from the above-cloud atmosphere that the cloud absorbs:

$$CF_{LW} \approx t_{bl}\varepsilon_c\sigma T_c^4 - t_{bl}\varepsilon_c\sigma T_a^4 = t_{bl}\varepsilon_c\sigma(T_c^4 - T_a^4). \tag{3}$$

Based on Arctic standard atmospheric profiles (Key 2001) of temperature, humidity, and downwelling LW flux, the effective temperature for the above-cloud atmosphere, T_a, at the cloud layer can be statistically determined from the cloud layer height. Due to the exponential decline of water vapor with height, the difference $\Delta T = T_c - T_a$ increases approximately linearly with height in the troposphere according to $\Delta T = 2.8z_c + 20$, where z_c is the cloud height in kilometers. Thus, T_a can be approximated from information on the cloud height.

Net surface SW fluxes under clear and cloudy skies can be approximated as

$$Q(0) = t_{bs}S\mu_0(1 - \alpha_s) = Q^{\downarrow}(1 - \alpha_s), \tag{4a}$$

$$Q(A_c) = t_{bs}S\mu_0(1 - \alpha_s)t_{cs} = Q^{\downarrow}(1 - \alpha_s)t_{cs}, \tag{4b}$$

where S is the solar constant, $\mu_0 = \cos\theta$, θ is the solar zenith angle, t_{bs} is the broadband atmospheric SW transmittance, α_s is the broadband surface albedo, t_{cs} is the broadband cloud SW transmittance (direct plus diffuse), and $Q\downarrow = t_{bs}S\mu_0$ is the downwelling clear-sky surface SW flux. The SW cloud transmittance is a complex function of cloud microphysical structure, solar zenith angle, and the surface albedo. Equations (4a) and (4b) assume that, to a first order, the variation of α_s with cloud fraction has a minimal impact. Thus, according to (1b), CF_{SW} is then

$$CF_{SW} \approx t_{bs}S\cos\theta(1 - \alpha_s)(t_{cs} - 1) = Q^{\downarrow}(1 - \alpha_s)(t_{cs} - 1). \tag{5}$$

Combining (1c), (3), and (5) yields a first-order approximation for the total CF:

$$CF \approx t_{bl}\varepsilon_c\sigma(T_c^4 - T_a^4) + t_{bs}S\mu_0(1 - \alpha_s)(t_{cs} - 1). \tag{6}$$

In summary, Eq. (6) reveals the major components that contribute to surface cloud forcing: cloud temperature and height, cloud microphysical composition, solar zenith angle, and surface albedo. Measurements from SHEBA are utilized to elucidate how each of these parameters participates in surface cloud forcing from an observational perspective. The SW and LW atmospheric transmittances also impact CF, however, they are not examined in depth here.

b. Calculations of surface cloud forcing

Surface cloud forcing was calculated on an hourly basis for the SHEBA year, using the definition of Ramanathan et al. (1989), as the measured net surface radiative flux minus the net flux had the skies been cloud free. Due to the ubiquitous presence of clouds in the Arctic, especially during the summer with monthly cloud fractions of ~90% (Intrieri et al. 2002b), a radiative transfer model was employed to calculate the clear sky fluxes instead of relying upon sporadic measurements of clear-sky conditions. Clear-sky LW and SW, upwelling and downwelling surface radiative fluxes were calculated using the Santa Barbara Discrete Ordinate Radiative Transfer (DISORT) Atmospheric Radiative Transfer (SBDART) algorithm (Ricchiazzi et al. 1998). Model inputs included hourly location of the SHEBA site, interpolated temperature and relative humidity soundings, and surface albedo calculated from the broadband radiometers. Since detailed aerosol measurements were not made at SHEBA, an SBDART standard maritime aerosol profile was assumed. Further de-

tails on the clear-sky model and surface cloud forcing calculations are available in Intrieri et al. (2002a). Annual cycle CF statistics are presented in 20-day averages because this time period retains the features of the annual cycle but smooths over synoptic weather events, extended clear-sky periods, and periodic instrument outages.

Uncertainty in the cloud forcing calculations arises from three sources—model uncertainties, measurement errors, and instrument mismatches. Due to these uncertainties, cloud forcing calculations for clear-sky conditions were distributed around 0 W m^{-2}. The CF_{SW} (CF_{LW}) mean and standard deviation under clear-sky conditions are 0 (6) and 8 (11) W m^{-2}, respectively. Therefore, we consider the uncertainty of the SW and LW cloud forcing calculations to be about 10 W m^{-2}. Of this total estimated uncertainty, Intrieri et al. (2002a) approximated the measurement-based errors in CF_{LW} and CF_{SW} to be about 3 W m^{-2} and 4.5%, respectively. Differences in instrument viewing scene contributed to the CF_{LW} bias under clear skies when the vertically pointing lidar/radar observed clear sky overhead but a cloud was observed in the hemispheric view of the radiometers.

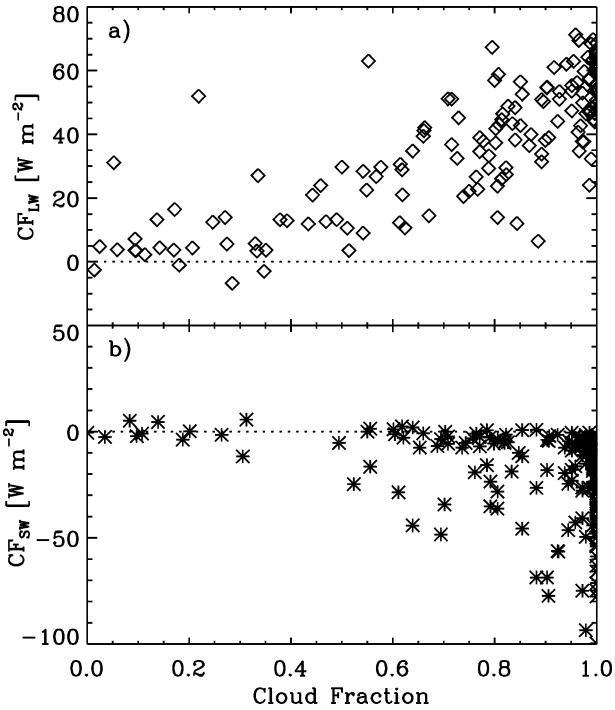

FIG. 2. Plot of (a) CF_{LW} and (b) CF_{SW} vs vertically pointing cloud fraction. The LW data are in 2-day averages, while SW data are in 1-day averages.

c. Surface cloud forcing sensitivity

To understand the implications of model/measurement uncertainties and potential changes in radiatively important parameters on the cloud radiative effect, we examine the sensitivity of CF to various cloud and environmental parameters. We define the sensitivity coefficient as the partial differential of a given forcing parameter with respect to a given cloud or environmental parameter. For example, $\partial CF_{LW}/\partial T_c$ is the sensitivity of CF_{LW} to cloud temperature. In effect, the sensitivity coefficient is the slope of the curve relating the two parameters at any given point. Sensitivity coefficients quantify the expected response of cloud forcing to changes in influential parameters, neglecting any feedbacks between parameters. Unfortunately, when using observational datasets, many parameters cannot be held fixed in order to establish the sensitivity to other parameters. When observational data cannot be used for these purposes, sensitivity parameters developed from the radiative forcing model described in section 3a are used to elucidate the expected impacts on CF from potential changes in radiatively important cloud and environment quantities.

4. Dependence of cloud forcing on cloud presence

There exist strong relationships between cloud fraction (defined from vertically pointing lidar and radar) over the permanent Arctic ice pack and both CF_{LW} and CF_{SW}. Two-day averages of A_c plotted against CF_{LW} (Fig. 2) show an increasing sensitivity to cloud presence as A_c increases. The sensitivity parameter [$\partial CF_{LW}/\partial A_c$; in units of watts per meter squared per percent cloudiness (W m^{-2} $\%^{-1}$)] increases from about 0.3 to 0.8 W m^{-2} $\%^{-1}$ across the range of observed cloud fraction with a mean of ~0.65 W m^{-2} $\%^{-1}$. Scatter in this relationship is due to variability in cloud microphysical composition and temperature, while the negative forcing values are attributed to clear-sky model errors. The strong sensitivity relationship suggests that an increase in cloudiness will substantially increase the amount of LW radiative warming at the Arctic surface, which was observed in the SHEBA measurements (Persson et al. 2002) and has been concluded by previous model studies (e.g., Curry et al. 1993). This positive correlation is the cloud greenhouse effect, which is particularly important in the Arctic due to the absence of solar energy for much of the year and because prevalent, low-level cloud layers often reside within strong temperature inversions.

The sensitivity of CF_{SW} to A_c is complicated over the course of the year because SW effects are, by nature, dependent upon the highly varying solar zenith angle and surface albedo. However, there is a general negative correlation, as illustrated in Fig. 2, where increased cloud cover causes a larger SW cooling effect at the surface. This negative correlation is the cloud albedo effect. The coefficient $\partial CF_{SW}/\partial A_c$ varies with solar zenith angle from 0 W m^{-2} $\%^{-1}$ when the sun is at or below the horizon to about 1.0 W m^{-2} $\%^{-1}$ when the sun is at a zenith angle between 55° and 65°. For higher

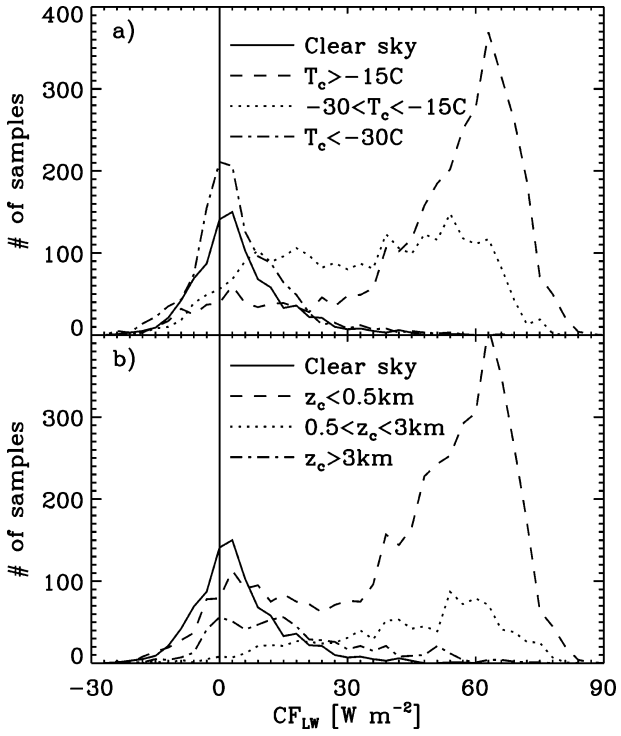

FIG. 3. Distributions of CF_{LW} distinguished by (a) cloud-base temperature and (b) cloud-base height. The clear-sky distribution (an uncertainty estimate for these calculations) is also shown in both (a) and (b).

sun elevations (i.e., in more southerly locations) this sensitivity will be larger.

The balance of $\partial CF_{LW}/\partial A_c$ and $\partial CF_{SW}/\partial A_c$ defines the net surface radiative response to changes in cloudiness. At SHEBA, $\partial CF_{LW}/\partial A_c$ was larger than $\partial CF_{SW}/\partial A_c$ for the majority of the year; thus, increases in cloudiness from current conditions would lead to a surface warming effect. Only in midsummer when the sun was highest in the sky did $\partial CF_{SW}/\partial A_c$ surpass $\partial CF_{LW}/\partial A_c$, indicating that increases in summer cloudiness would cool the surface. At lower latitudes, with higher sun elevations, $\partial CF_{SW}/\partial A_c$ will be larger than $\partial CF_{LW}/\partial A_c$ for a longer portion of the year. The hinge point at which the SW sensitivity outweighs the LW sensitivity is clearly linked to the availability of solar energy in addition to other factors such as surface albedo and cloud properties.

5. The components of LW surface cloud forcing

The LW radiative properties of clouds are primarily determined by cloud temperature, height, and emissivity (or microphysical properties).

a. Cloud temperature and height

When considering cloud temperature, the role of frequent low-level Arctic temperature inversions is particularly important since low clouds often reside at temperatures greater than the underlying surface. Figure 3 shows distributions of CF_{LW} for the entire SHEBA year that are distinguished by different temperature and height ranges. A distribution of CF_{LW} for conditions identified as clear sky by the vertically pointing instruments is also provided and reveals the uncertainty in forcing calculations due to model and measurement errors. Clouds warmer than −15°C are primarily responsible for the largest CF_{LW} values, while clouds colder than −30°C are most often indistinguishable from clear skies. Intermediate temperature clouds show a range of CF_{LW} from around 0 to greater than 60 W m^{-2}. In terms of cloud height (Fig. 3b), the largest positive CF_{LW} values correspond with cloud scenes based below 0.5 km. The apparent decrease in CF_{LW} with height is deceptive in that it is mostly due to the related cloud temperature effect. According to (3), CF_{LW} actually increases with cloud height for a constant cloud temperature. This forcing increase is due to a decrease in the above-cloud atmospheric flux that is absorbed by the cloud (i.e., the above-cloud effective temperature decreases with height), while the cloud emission term is nearly unchanged. Two cloud height ranges show distribution modes that are similar to the CF_{LW} distribution for clear skies: high clouds above 3 km and low clouds below 0.5 km. The high-cloud component demonstrates the manner in which lower temperatures, and often lower emissivities, at higher altitudes produce a weak CF_{LW}. The low-level component is somewhat more surprising. These clouds are typically diamond dust (ice crystal layers that extend down to the surface) that are within a few degrees of the surface temperature but have very low emissivities. Thus, these data indicate that diamond dust does not have a significant impact on the surface radiation balance over the Arctic ice pack. A more detailed analysis of the diamond dust observations at SHEBA is provided by Intrieri and Shupe (2003, manuscript submitted to *J. Climate*).

Based on the data shown in Fig. 3, a CF_{LW} threshold can be identified below which clouds are considered radiatively insignificant (or indistinguishable from clear skies) in the LW. The mean CF_{LW} under clear sky conditions is 6.3 W m^{-2}; thus, we only consider forcings greater than this value to be significant. The positive bias in CF_{LW} under clear sky conditions is primarily due to partial cloudiness that is not detected by the vertically pointing instruments (i.e., classified as clear sky) but is detected by the hemispheric radiometers. Of the radiatively significant cloud scenes, 80% had bases below 1 km and temperatures warmer than −23°C. Ninety-five percent of the radiatively significant cloud scenes were based below 4.3 km with temperatures warmer than −31°C. By season, 95% of the radiatively important clouds had base temperatures above −36°C in winter (November–February), −30°C in spring (March–May), and −10°C in summer (June–September).

The CF_{LW} becomes more sensitive to T_c as T_c, cloud emissivity, and cloud height increase. Increases in the first two parameters cause the cloud emission term in

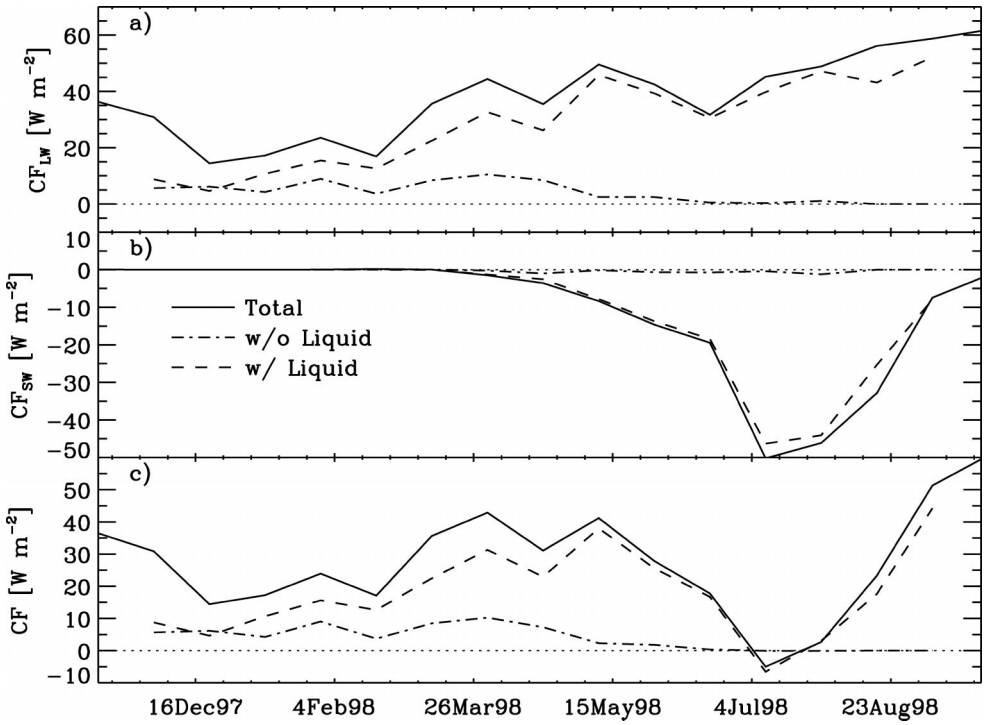

FIG. 4. Twenty-day averaged annual cycles of (a) CF_{LW}, (b) CF_{SW}, and (c) total CF for all cloud scenes, for those containing liquid and for those with only ice. The curves partitioned by cloud type are weighted by cloud fraction. The dotted line shows CF = 0 W m^{-2}.

(3) to be more dominant, while increases in cloud height cause the upper-atmosphere emission term to be less dominant. In each case, the cloud emission term increases in relative importance such that the LW forcing is more sensitive to changes in cloud emission. Under typical Arctic conditions (with black clouds at $\varepsilon_c \approx 1$), the cloud temperature sensitivity coefficient, $\partial CF_{LW}/\partial T_c$, has an average value of about 1 W m^{-2} (°C)$^{-1}$ over the typical range of cloud temperatures. The sensitivity of CF_{LW} to cloud height is also positive, but decreases with altitude due to the same argument as for T_c, albeit in the opposite direction. To place these results in the context of potential cloud changes, consider a black cloud at 4 km, $T_c = 0$°C, and $t_{bl} = 0.7$. Under these circumstances a 1°C increase in T_c or a 0.15 km increase in cloud height will lead to a 1 W m^{-2} increase in CF_{LW}. These types of changes in cloud properties are possible and likely in response to changes in global and regional temperature, circulation, and/or dynamics.

b. Cloud phase and microphysics

Cloud phase in and of itself does not directly control CF_{LW}; the absolute relationship between particle size and CF_{LW} is similar for both liquid drops and ice crystals (Francis 1999). However, phase does play an important indirect role in that it defines cloud microphysical composition. Ice particles are typically larger than liquid droplets but have a smaller relative mass density and occur in smaller concentrations.

The annual cycle of 20-day average CF_{LW} is shown in Fig. 4a along with the contributions to this total from cloud scenes containing liquid water and those containing only ice. Liquid-containing cloud scenes are the dominant LW radiative component in all seasons except the middle of winter, when ice-only cloud scenes have a similar LW contribution. These annual cycles suggest that there is a higher fraction of ice-only clouds in the winter (Intrieri et al. 2002b) and that the difference in cloud emissivity between cloud types is smaller in the winter (i.e., winter liquid clouds have lower LWPs). In no season do the ice-only clouds contribute more than 10 W m^{-2} to the mean LW forcing.

Distributions of CF_{LW} for liquid-containing cloud scenes, ice-only cloud scenes, and clear skies are shown in Fig. 5a. The distribution of CF_{LW} for ice-only cloud scenes is similar to the distribution for clear skies (discussed above). However, the distribution for liquid-containing cloud scenes shows a strong LW warming effect at the surface. The slight skewness to the ice-only distribution suggests that some optically thicker ice clouds do have a significant warming effect. Annual mean CF_{LW} values are 52, 16, and 6 W m^{-2} for liquid-containing, ice-only, and clear-sky conditions. The bias of CF_{LW} under clear-sky conditions provides an uncertainty estimate for the forcing values computed in this manner.

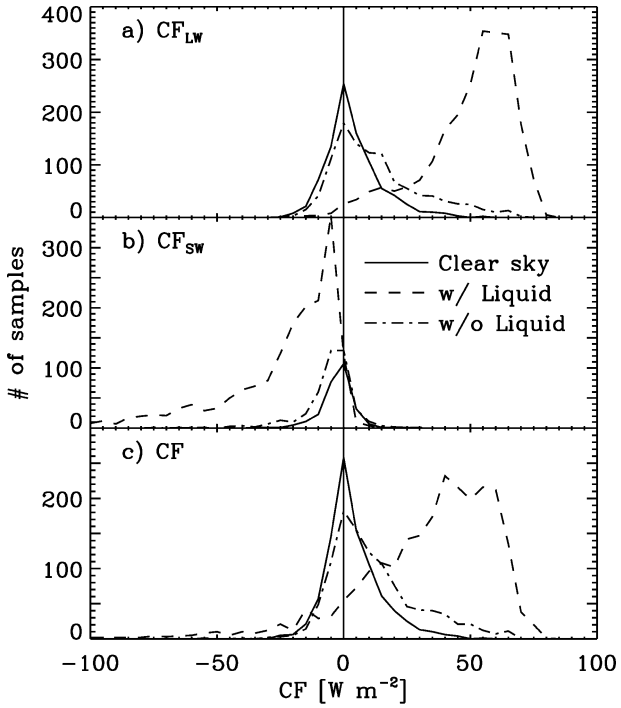

FIG. 5. Distributions of (a) CF_{LW}, (b) CF_{SW}, and (c) total CF partitioned into cloud scenes containing liquid, those with only ice, and clear-sky time periods.

Both Figs. 4a and 5a indicate the strong role of cloud phase in the surface LW radiative balance. Specifically, the presence of liquid water significantly increases the cloud LW greenhouse warming effect. As is evident in (3), the manner in which cloud phase, and thus microphysics, contributes to CF_{LW} is through cloud emissivity. Stephens (1978) parameterized the downwelling broadband LW cloud emissivity as

$$\varepsilon_c = 1 - e^{-a_o \mathrm{LWP}}, \tag{7}$$

where a_o is the total IR flux mass absorption coefficient, and the particle size is assumed to be related to LWP. Other studies have parameterized the exponential component of (7), or the optical depth, in terms of both LWP and particle size (e.g., Curry and Herman 1985). We acknowledge the importance of cloud particle size but do not specifically address it here and instead utilize (7) since we have direct retrievals of LWP from the MWR. Equation (7) does not adequately describe the emissivity of all-ice clouds, but is appropriate for the most radiatively significant (liquid-containing) cloud scenes observed at SHEBA.

The observed relationship between cloud microphysics (expressed in terms of LWP) and CF_{LW} is shown in Fig. 6a. The CF_{LW} increases with LWP until LWP = 30 g m^{-2}, after which point clouds emit as blackbodies ($\varepsilon_c \cong 1$), and increasing LWP has no further impact on

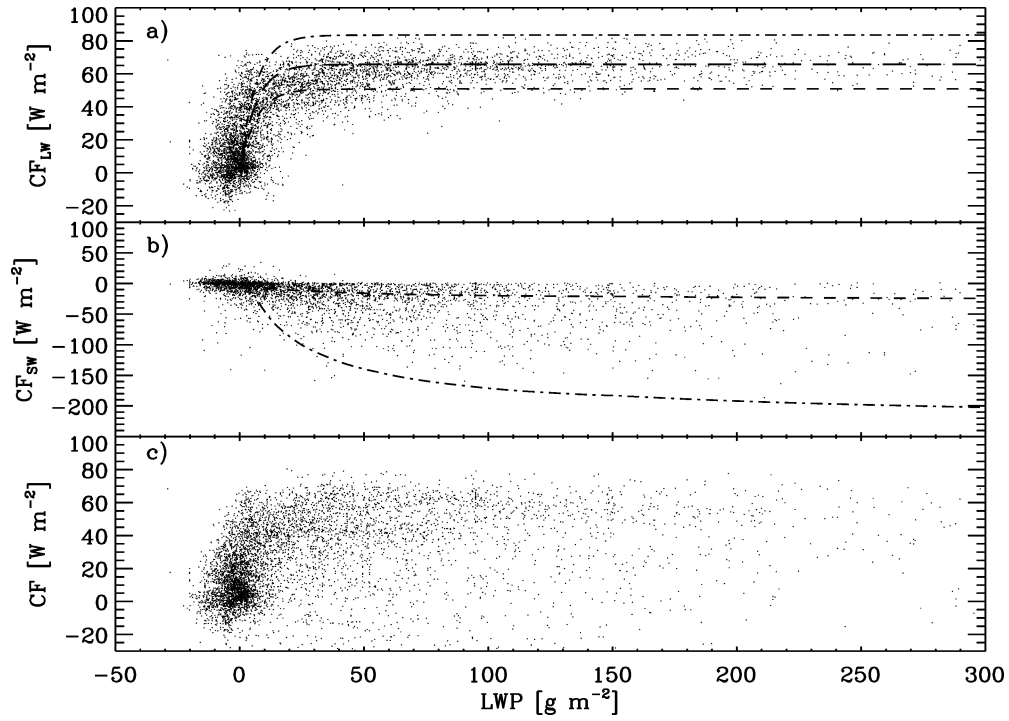

FIG. 6. Observed relationship between MWR-derived LWP and (a) CF_{LW}, (b) CF_{SW}, and (c) CF. Curves in (a) are derived from Eq. (3) using typical cloud temperatures of 0° (dash–dot), −20° (long dash), and −40°C (short dash). Cloud base and LW atmospheric transmittance were assumed to be 1 km and 0.9, respectively. Curves in (b) are derived from Eq. (5) for typical spring (short dash) and midsummer (dash–dot) conditions using values for θ, α_s of 80°, 0.8 and 60°, 0.5 respectively.

downwelling LW radiation. Scatter in Fig. 6a is due to variations in cloud phase, temperature, height, and hydrometeor size. Nearly all observations with small CF_{LW} (± 20 W m^{-2}) contain insignificant amounts of liquid water (i.e., less than the MWR LWP uncertainty). The curves in Fig. 6a are based on (3), utilizing (7), and are specified to represent a typical range of cloud temperatures observed at SHEBA ($T_c = -40°$, $-20°$, and 0°C) for a cloud at 1 km. The comparison of the observational data with these theoretical curves, which were defined to roughly bound the observational data, suggests that (3) is a reasonable approximation for CF.

The sensitivity of CF_{LW} to LWP decreases as LWP increases and goes to zero at LWP ≥ 30 g m^{-2}. This LW saturation effect has been noted often in the literature. Unfortunately, due to the retrieval uncertainty of the MWR, we do not have adequate measurements of LWP in the high-sensitivity regime below 25 g m^{-2}. From (3) and (7), we see that $\partial CF_{LW}/\partial LWP$ is also proportional to the fourth power of T_c and cloud height. Thus, changes in LWP are most important in high, optically thin yet relatively warm clouds, such as the frequent Arctic winter mixed-phase clouds that reside within a strong temperature inversion.

6. The components of SW cloud forcing

In many respects, Arctic CF_{SW} is more complex than its LW counterpart. Scattering by cloud particles is more important in the SW, and multiple scattering between the surface and cloud layers amplifies the cloud SW contribution, particularly over a highly reflective surface. Furthermore, the solar zenith angle changes on both diurnal and seasonal time scales, greatly impacting the total solar radiation that is available to interact with cloud layers.

a. Cloud phase and microphysics

Cloud phase has a larger direct influence on SW radiation than on LW radiation due to the difference in SW scattering properties between spherical water droplets and nonspherical ice crystals. The annual cycles of CF_{SW} in Fig. 4b show that cloud scenes containing liquid strongly dominate the SW cloud albedo effect in all sunlit seasons and that ice-only cloud scenes have very little SW shading effect.

Distributions of CF_{SW} for time periods when the sun was above the horizon (Fig. 5b) also demonstrate that liquid-containing cloud scenes are responsible for the periods of significant SW surface cooling. Due to low sun angles during much of the polar ''day,'' the majority of liquid-containing cloud scenes cause only a weak SW cooling at the surface. During the higher insolation midsummer months, the liquid-containing cloud scenes cool the surface by as much as 100 W m^{-2} with respect to clear skies. The annual mean CF_{SW} from liquid-containing cloud scenes is about -21 W m^{-2}. Distributions of CF_{SW} for all-ice and clear-sky conditions are both centered near zero forcing with the all-ice clouds cooling the surface by an average of -3 W m^{-2}. The CF_{SW} distribution for clear-sky periods provides an estimate of the uncertainty in computing the forcing in this manner.

Both Figs. 4b and 5b clearly indicate that liquid-containing clouds cool the surface more than ice clouds. In other words, liquid cloud scenes have a higher albedo than all-ice cloud scenes. Model studies by Francis (1999) suggest that this is due to a size effect rather than a phase effect since model results actually show larger cooling for ice particles than liquid droplets of the same size. The liquid clouds observed at SHEBA cool more effectively because they are composed of many small droplets instead of relatively few large ice crystals, and thus have a greater surface area per volume, giving them a higher optical depth and a lower transmittance.

The cloud SW transmittance is a function of cloud microphysical properties, the zenith angle, and the surface reflectance. Thus, t_{cs} includes the net radiative interactions between cloud and surface by taking into account the direct transmittance of radiation by the cloud, multiple reflections between the cloud and surface, and the transmittance of radiation back through the cloud layer on each reflection from the surface. Cloud transmittance has been parameterized in terms of LWP by Stephens (1978) and modified by Stephens et al. (1984) under the assumption that particle size is inherently parameterized via the LWP. Various authors (e.g., Slingo 1989; Ebert and Curry 1993) have parameterized the SW optical depth (and, thus, transmittance) in terms of both LWP and particle size. Here, we utilize the one-parameter relationship of Stephens (1978) since we do not have explicit observational information on particle size.

The magnitude of CF_{SW} typically increases with LWP (Fig. 6b) and cloud scenes with little LWP (i.e., mostly ice) have only a small cooling effect. Observations near $CF_{SW} = 0$ W m^{-2} at higher values of LWP are due to low sun angles while the SW cooling effect increases when the sun is higher in the sky. For comparison, two curves are calculated using (5) and the Stephens (1978) cloud transmittance parameterization. The curves are intended to place crude boundaries on the expected spread of the data with the upper and lower curves corresponding to characteristic days of early spring ($\theta = 80°$ and $\alpha = 0.8$) and the middle of summer ($\theta = 60°$ and $\alpha_s = 0.5$), respectively. The fact that the two curves bound the data suggests that (5) is a reasonable approximation for CF_{SW}.

The sensitivity of CF_{SW} to cloud microphysics is particularly important for thick clouds because clouds become optically opaque in the SW at higher values of LWP than in the LW. Thus, as LWP increases, the cloud SW shading effect continues to increase after the LW greenhouse effect becomes saturated. Due to the com-

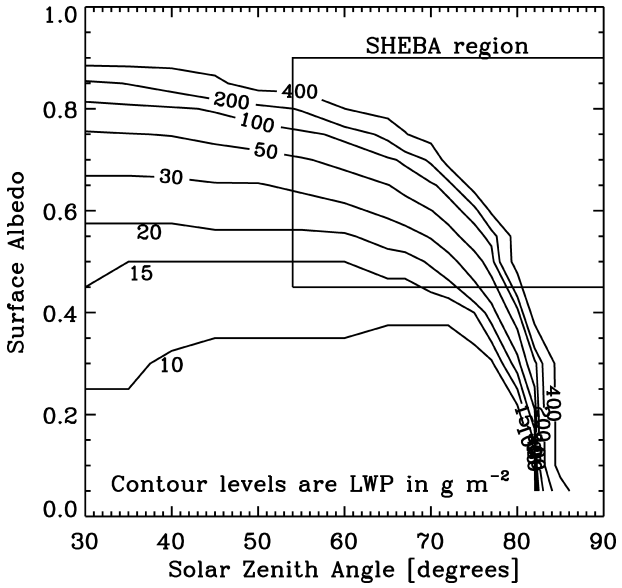

FIG. 7. Contours of the cloud LWP value at which point the SW surface cloud cooling effect becomes dominant over the LW warming effect as a function of θ and α_s. The following parameters are assumed: $T_c = -10°C$, $z_c = 1$ km, $t_{al} = 0.9$, and $t_{as} = 0.75$.

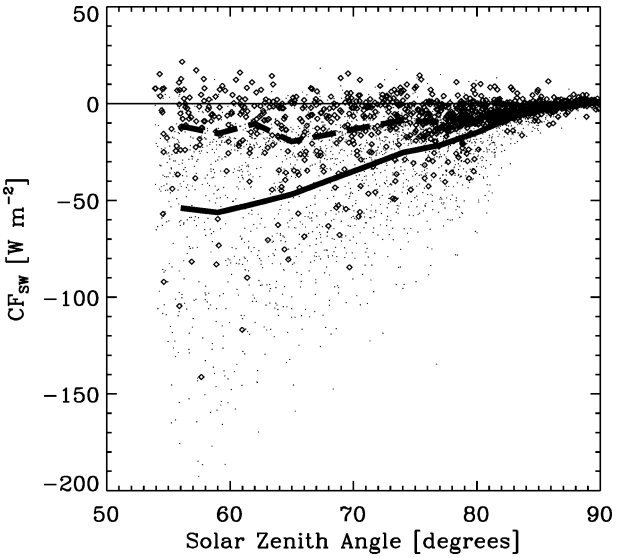

FIG. 8. The relationship of solar zenith angle with CF_{SW} for cloud scenes with liquid (dots, solid line) and without liquid (diamonds, dashed line). The curves show average relationships between these parameters in 3° bins.

plexity of the LWP–t_{cs} relationship over a reflective surface, computing $\partial CF_{SW}/\partial LWP$ directly is difficult. Equation (5) and Fig. 6b suggest that this sensitivity is inversely proportional to α_s and LWP and directly proportional to μ_0. Thus, as the surface albedo decreases, the sun becomes higher in the sky, and/or the clouds thin, CF_{SW} becomes more sensitive to cloud microphysical composition.

Cloud optical depth is a particularly important parameter because it influences both of the competing CF_{SW} and CF_{LW}. Here we use LWP as a surrogate for optical depth. At some LWP the cloud SW cooling effects surpass the LW warming effects for a given combination of θ, α_s, T_c, and z_c. Figure 7 shows contours of this crossover LWP value versus θ and α_s, calculated from (6) and the Stephens (1978) parameterizations, for a typical Arctic cloud at 1 km and $-10°C$. At SHEBA, θ ranged from $>90°$ to 54°, and α_s ranged from 0.9 to 0.45. The LWP crossover value increases as both θ and α_s increase. At warmer cloud temperatures or higher cloud heights, the LWP crossover point also increases (not shown). For $\theta < 40°$ (i.e., at lower latitudes than SHEBA), the crossover point becomes insensitive to sun angle. For $\theta > 70°$, the solar insolation rapidly decreases causing the cloud SW cooling effects to quickly decrease. These decreases in turn cause the LWP crossover value to increase to levels that are unreasonably high for Arctic clouds (i.e., typical clouds will have a warming effect). Interestingly, at low α_s all contour lines tend to converge at a sun angle between 80° and 85°, which may explain the statement made by Minnett (1999) that the shift from cloud warming to cooling occurs at about 80° as θ decreases. According to Fig. 7, this is true for a surface albedo less than about 0.4, which was likely the case for Minnett's observations in an ocean environment with broken sea ice. As α_s increases, the crossover sun angle becomes increasingly dependent upon the cloud LWP. Thus, Minnett's analysis is applicable only for surface conditions and sun angles similar to those encountered during the Arctic summer northeast of Greenland. If the transition from cloud warming to cooling occurred at 80°, independent of other parameters, the SHEBA location would have experienced a cloud cooling effect for at least one-half of the day for 22 April–29 August and for the full day for 11 June–16 July. These trends were not observed (see Fig. 4).

b. Solar zenith angle and the diurnal cycle

The solar zenith angle contributes significantly to diurnal and seasonal variations of Arctic CF. Figure 8 shows a scatterplot of θ versus CF_{SW} for cloud scenes containing liquid and those containing no liquid, as well as the average CF_{SW} over 3° wide bins for both of these cloud scene types. For both cloud types, the SW shading effect increases as the sun rises in the sky. At the highest sun angles observed at SHEBA, average cooling for all-ice and liquid-containing cloud scenes was -15 and -55 W m^{-2}, respectively. The relationship between θ and CF_{SW} suggests that as the SHEBA site drifted northward, the relative contribution of the cloud SW cooling effect decreased. The total change in zenith angle during the sunlit months along the SHEBA drift track was about 5°. Had the observation site remained farther to the south, the CF_{SW} values reported here would have been,

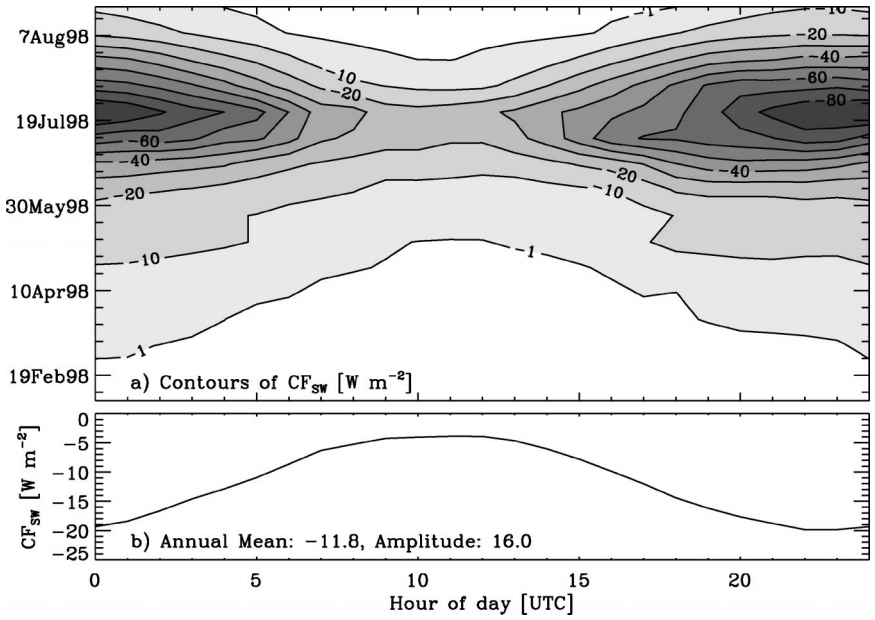

FIG. 9. (a) Contours of CF_{SW} showing the evolution of the diurnal cycle with date and (b) the annual mean CF_{SW} diurnal cycle. Resolutions are 1 h for the diurnal cycle and 2 weeks for the annual evolution. The annual mean and annual diurnal-cycle amplitude are inset in (b).

on average, larger by 3–4 W m^{-2} in the middle of the summer and by as much as 8 W m^{-2} in the fall. Thus, at lower latitudes, we expect the period in summer when clouds have a net cooling effect on the surface (Fig. 4c) to be longer.

The maximum CF_{SW} at a given time is dependent on the insolation. We define the cloud forcing fraction, CFF, as the ratio of CF_{SW} to TOA insolation. In a mean sense for the SHEBA location and conditions, the CFF for liquid-containing cloud scenes was ~10%, and was somewhat less for ice-only scenes (~3%). The upper bound on CFF at SHEBA was about 25%. This upper limit is due to the maximum LWP and the minimum α_s observed at SHEBA. These percentages can be used to scale the expected CF_{SW} to the insolation at a given latitude, assuming cloud and surface properties are similar to those observed at SHEBA.

Closely tied to θ are the diurnal variations in surface radiation and CF. Net surface SW and LW fluxes had annual-mean diurnal cycle variations of 54 and 5 W m^{-2}, respectively. In terms of forcing, the CF_{SW} (Fig. 9b), CF_{LW}, and CF had annual-mean diurnal cycle amplitudes of 16, 3, and 19 W m^{-2}, respectively. Note that there was no significant diurnal cycle in cloudiness that would have impacted the diurnal cycle of CF. The months of November through February showed no diurnal cycle of CF_{SW} since there was virtually no insolation during those months. Starting in March, the amplitude of the CF_{SW} diurnal cycle increased monotonically (following the increase in daily average SW cooling) until the middle of July after which the amplitude again decreased (Fig. 9a). Since the maximum diurnal cycle amplitude of SW flux occurred in June, it is clear that other factors (i.e., α_s) also contributed to the diurnal cycle of CF_{SW}. Throughout the sunlit months, the minimum diurnal CF_{SW} cooling effect occurred near solar midnight (~1100 UTC), and the maximum cooling occurred near solar noon (~2200 UTC). In other words, the shading effect of clouds is strongest when the sun is highest in the sky.

c. Surface albedo

The annual minima of CF_{SW} and α_s occurred at nearly the same time at SHEBA. Thus, the interactions of clouds, radiation, and α_s clearly play an important role in the surface energy balance, formally called the ice–albedo feedback. Over the SHEBA annual cycle, α_s (calculated from radiometer measurements) ranged from roughly 0.9 in the winter to a minimum of about 0.45 in the late summer (Persson et al. 2002). As the albedo decreased, the CF_{SW} cooling effect increased steadily because relatively more SW radiation was absorbed by the surface under clear skies. The sensitivity of CF_{SW} to α_s, $\partial CF_{SW}/\partial\alpha_s$, is inversely related to t_{cs}, α_s, and θ. Thus, the sensitivity increases from the winter to the summer as each of t_{cs}, α_s, and θ decreases. For typical late-spring Arctic conditions ($\theta = 60°$, $\alpha_s = 0.6$, LWP = 50 g m^{-2}), a decrease in the surface albedo of 0.1 will cool the surface by about 40 W m^{-2} in the SW, constituting a negative radiative feedback.

7. Summary

An annual cycle of surface-based observations are utilized to identify the radiatively important properties

of Arctic clouds over multiyear sea ice. Cloud phase, microphysics, temperature, and height are each radiatively important in the surface energy balance and have been examined here. Additionally, the indirect impacts of solar zenith angle and surface albedo have been addressed. The analysis is based on cloud and radiation measurements made as part of the SHEBA program in the Beaufort and Chukchi Seas during 1997–98. Cloud radiative forcing, defined as the net radiation under all skies minus the net radiation under clear skies, was calculated for the SHEBA annual cycle and reported by Intrieri et al. (2002a). The cloud forcing dataset is explored further in this study to distinguish and examine the properties of clouds that are most radiatively important. A first-order radiative flux model is used to illustrate these radiatively important parameters. When possible, the sensitivity of cloud radiative impacts to pertinent parameters is also discussed in order to assess how the cloud–radiation interaction may respond to potential changes in these parameters. Results presented here cover an annual cycle (the first dataset of its type in the Arctic) for a site that drifted in the western Arctic basin. These results will not necessarily characterize the entire Arctic region nor be representative of all years; however, the authors feel it is a reasonable description of how clouds influence the surface radiative balance of the permanent ice pack of the Arctic Ocean. Major conclusions presented here include:

- Surface cloud forcing is a complex function of cloud properties (phase, optical depth, LWP, particle size, emitting temperature, height), solar zenith angle, and surface albedo.
- The sensitivity of CF_{LW} to cloud fraction is approximately linear with an average sensitivity coefficient of 0.65 W m^{-2} per percent cloudiness. The sensitivity of CF_{SW} to cloud presence is dependent on the total insolation, varying from 0 under no insolation to about 1.0 W m^{-2} per percent cloudiness under the highest insolation observed at SHEBA. An increase in cloudiness will impart greater surface warming relative to current conditions for most of the annual cycle, when LW effects are stronger, but will enhance surface cooling for a few weeks in midsummer, when SW shading effects are stronger.
- Ninety-five percent of LW radiatively important cloud scenes had bases below 4.3 km. During the winter, spring, and summer, 95% of the radiatively important cloud scenes had base temperatures warmer than $-36°$, $-30°$, and $-10°$C, respectively. The Arctic LW radiative balance is strongly impacted by frequent temperature inversions.
- The CF_{LW} increases with T_c, and the sensitivity of CF_{LW} to cloud temperature is about 1 W m^{-2} °C^{-1} for optically thick clouds at typical Arctic cloud temperatures.
- The CF_{LW} is particularly sensitive to LWP for LWP < 30 g m^{-2} but insensitive to higher LWPs, at which point clouds act as blackbody emitters.
- Cloud SW transmittance and the sensitivity of CF_{SW} to LWP both decrease as LWP increases, but there is less of a saturation effect than is seen in the LW.
- The LWP crossover point where SW cloud cooling effects surpass LW warming effects increases as θ, α_s, T_c, and z_c increase. At SHEBA, the crossover point was typically at unreasonably high values of LWP (>400 g m^{-2}) except in midsummer (low θ and α_s) when the crossover threshold reached below 20 g m^{-2}.
- The maximum CF_{SW} is limited by the TOA insolation; CF_{SW} was at most 25% of the insolation and, on average, 10% for liquid-containing and 3% for ice-only cloud scenes.
- Cloud SW shading effects increase with sun elevation.
- Surface CF_{SW} undergoes an annually averaged diurnal cycle, ranging from no cycle in the winter (no sun) to a maximum monthly averaged diurnal amplitude of about 60 W m^{-2} in July. The minimum diurnal SW cloud cooling effect occurs near solar midnight, and the maximum daily cooling occurs near solar noon.
- Cloud induced SW surface cooling increases with decreasing surface albedo.

In summary, the results presented here demonstrate that low-level liquid clouds are dominant in the radiative balance of a multiyear sea ice surface, while ice clouds of any type, including diamond dust, are not as important. Liquid clouds are the significant factor in the overall positive cloud forcing (LW warming) that occurs over most of the year, acting as insulating layers that trap the earth's radiation. These same clouds are also predominantly responsible for the negative forcing (SW cooling) that occurs for a few weeks in the middle of summer when the sun is highest in the sky, and the surface albedo is at its annual minimum. Cloud liquid can occur with relatively high, and previously unexpected, frequency in the winter and be present at temperatures as low as $-35°$C and up to 6.5 km in altitude (Intrieri et al. 2002b). Since many models currently parameterize liquid presence and amount as a function of temperature above a given threshold (e.g., $-22°$C in the model of Curry and Ebert 1992), the important radiative contributions of thin, wintertime liquid layers may be incorrectly represented and/or falsely attributed to diamond dust. Future work in the field of Arctic clouds and radiation will be greatly facilitated by the placement of depolarization lidars at key Arctic locations as well as improvements to liquid water retrievals from microwave radiometers.

Acknowledgments. This research was supported by the Biological and Environmental Research Program (BER), U.S. Department of Energy, Interagency Agreement DE-AI03-02ER63325, the NSF SHEBA Agreement OPP-9701730, and the NASA FIRE-ACE Contract L64205D. Microwave radiometer data were obtained

from the U.S. DOE Atmospheric Radiation Measurement Program. Radiosonde data were obtained from the University of Washington, Applied Physics Laboratory. Special thanks to Taneil Uttal, Sergey Matrosov, Chris Fairall, the SHEBA team, and the crew of the Canadian Coast Guard Ship *Des Grosseilliers.*

REFERENCES

Alvarez, R. J., II, W. L. Eberhard, J. M. Intrieri, C. J. Grund, and S. P. Sandberg, 1998: A depolarization and backscatter lidar for unattended operation in varied meteorological conditions. Preprints, *10th Symp. on Meteorological Observations and Instrumentation,* Phoenix, AZ, Amer. Meteor. Soc., 140–144.

Chen, B., D. H. Bromwich, K. M. Hines, and X. Pan, 1995: Simulations of the 1979–1988 polar climates by global climate models. *Ann. Glaciol.,* **21,** 85–90.

Cogley, J. G., and A. Henderson-Sellers, 1984: Effects of cloudiness on the high-latitude surface radiation balance. *Mon. Wea. Rev.,* **112,** 1017–1032.

Curry, J. A., and G. F. Herman, 1985: Infrared radiative properties of summertime Arctic stratus clouds. *J. Climate Appl. Meteor.,* **24,** 526–538.

——, and E. E. Ebert, 1992: Annual cycle of radiative fluxes over the Arctic Ocean: Sensitivity to cloud optical properties. *J. Climate,* **5,** 1267–1280.

——, J. L. Schramm, and E. E. Ebert, 1993: Impact of clouds on the surface radiation balance of the Arctic Ocean. *Meteor. Atmos. Phys.,* **51,** 197–217.

——, W. B. Rossow, D. Randall, and J. L. Schramm, 1996: Overview of Arctic cloud and radiation characteristics. *J. Climate,* **9,** 1731–1764.

Ebert, E. E., and J. A. Curry, 1993: An intermediate one-dimensional thermodynamic sea ice model for investigating ice–atmosphere interactions. *J. Geophys. Res.,* **98,** 10 085–10 109.

Francis, J., 1999: Cloud radiative forcing over Arctic surfaces. Preprints, *Fifth Conf. on Polar Meteorology and Oceanography,* Dallas, TX, Amer. Meteor. Soc., 221–226.

Intrieri, J. M., C. F. Fairall, M. D. Shupe, O. G. P. Persson, E. L Andreas, P. Guest, and R. M. Moritz, 2002a: An annual cycle of Arctic surface cloud forcing at SHEBA. *J. Geophys. Res.,* **107**, 8039, doi:10.1029/2000JC000439.

——, M. D. Shupe, T. Uttal, and B. J. McCarty, 2002b: An annual cycle of Arctic cloud characteristics observed by radar and lidar at SHEBA. *J. Geophys. Res.,* **107**, 8030, doi:10.1029/2000JC000423.

Key, J., 2001: Streamer user's guide. Cooperative Institute for Meteorological Satellite Studies, University of Wisconsin—Madison, 96 pp.

Maykut, G. A., and N. Untersteiner, 1971: Some results from a time-dependent thermodynamic model of sea ice. *J. Geophys. Res.,* **76,** 1550–1575.

Meehl, G. A., and W. M. Washington, 1990: CO_2 climate sensitivity and snow–sea–ice albedo parameterization in an atmospheric GCM coupled to a mixed layer ocean model. *Climatic Change,* **16,** 283–306.

Miller, J. R., and G. L. Russell, 2002: Projected impact of climate change on the energy budget of the Arctic Ocean by a global climate model. *J. Climate,* **15,** 3028–3042.

Minnett, P. J., 1999: The influence of solar zenith angle and cloud type on cloud radiative forcing at the surface in the Arctic. *J. Climate,* **12,** 147–158.

Moran, K. P., B. E. Martner, M. J. Post, R. A. Kropfli, D. C. Welsh, and K. B. Widener, 1998: An unattended cloud-profiling radar for use in climate research. *Bull. Amer. Meteor. Soc.,* **79,** 443–455.

Perovich, D. K., and Coauthors, 1999: The surface heat budget of the Arctic Ocean. *Eos, Trans. Amer. Geophys. Union,* **80,** 481–486.

Persson, P. O. G., C. W. Fairall, E. L Andreas, P. Guest, and D. Perovich, 2002: Measurements near the Atmospheric Surface Flux Group tower at SHEBA: Near-surface conditions and surface energy budgets. *J. Geophys. Res.,* **107**, 8045, doi:10.1029/2000JC000705.

Ramanathan, V., R. D. Cess, E. F. Harrison, P. Minnis, B. R. Barkstrom, E. Ahmad, and D. Hartman, 1989: Cloud–radiative forcing and climate: Results for the Earth Radiation Budget Experiment. *Science,* **243,** 57–63.

Ricchiazzi, P., W. Yang, C. Gautier, and D. Sowle, 1998: SBDART: A research and teaching software tool for plane-parallel radiative transfer in the earth's atmosphere. *Bull. Amer. Meteor. Soc.,* **79,** 2101–2114.

Schweiger, A. J., and J. R. Key, 1994: Arctic Ocean radiative fluxes and cloud forcing estimates from the ISCCP C2 cloud dataset, 1983–1990. *J. Appl. Meteor.,* **33,** 948–963.

Slingo, A., 1989: A GCM parameterization for the shortwave radiative properties of water clouds. *J. Atmos. Sci.,* **46,** 1419–1427.

Smith, W. L., X. L. Ma, S. A. Ackerman, H. E. Revercomb, and R. O. Knuteson, 1993: Remote sensing cloud properties from high spectral resolution infrared observations. *J. Atmos. Sci.,* **50,** 1708–1720.

Stephens, G. L., 1978: Radiation profiles in extended water clouds. II: Parameterization schemes. *J. Atmos. Sci.,* **35,** 2123–2132.

——, S. Ackerman, and E. A. Smith, 1984: A shortwave parameterization revised to improve cloud absorption. *J. Atmos. Sci.,* **41,** 687–690.

Stokes, G. M., and S. E. Schwartz, 1994: The Atmospheric Radiation Measurement (ARM) Program: Programmatic background and design of the cloud and radiation test bed. *Bull. Amer. Meteor. Soc.,* **75,** 1201–1221.

Tao, X., J. E. Walsh, and W. L. Chapman, 1996: An assessment of global climate model simulations of Arctic air temperatures. *J. Climate,* **9,** 1060–1076.

Uttal, T., and Coauthors, 2002: Surface Heat Budget of the Arctic Ocean. *Bull. Amer. Meteor. Soc.,* **83,** 255–275.

Walsh, J. E., and W. L. Chapman, 1998: Arctic cloud–radiation–temperature associations in observational data and atmospheric reanalyses. *J. Climate,* **11,** 3030–3044.

——, V. M. Kattsov, W. L. Chapman, V. Govorkova, and T. Pavlova, 2002: Comparison of Arctic climate simulations by uncoupled and coupled global models. *J. Climate,* **15,** 1429–1446.

Westwater, E. R., Y. Han, M. D. Shupe, and S. Y. Matrosov, 2001: Analysis of integrated cloud liquid and precipitable water vapor retrievals from microwave radiometers during SHEBA. *J. Geophys. Res.,* **106,** 32 019–32 030.

Zhang, T., K. Stamnes, and S. A. Bowling, 1996: Impact of clouds on surface radiative fluxes and snow melt in the Arctic and subarctic. *J. Climate,* **9,** 2110–2123.